*Journal of Polymers and the Environment, Vol. 13, No. 2, April 2005 (© 2005)*
DOI: 10.1007/s10924-005-2940-1

# Biobased Epoxy/Layered Silicate Nanocomposites: Thermophysical Properties and Fracture Behavior Evaluation

**Hiroaki Miyagawa,[1] Manjusri Misra,[1] Lawrence T. Drzal,[1] and Amar K. Mohanty[2,3]**

The biobased epoxy containing epoxidized linseed oil (ELO) and its clay nanocomposites were processed with an anhydride curing agent. The certain amount of diglycidyl ether of bisphenol F (DGEBF) was replaced by ELO. The selection of the DGEBF, ELO, an anhydride curing agent, and organo-montmorillonite clay resulted in an excellent combination, to provide new biobased epoxy/clay nanocomposites showing high elastic modulus, high glass transition temperature, and high fracture toughness with larger amount of ELO. Izod impact strength was almost constant while changing the amount of ELO. This is a promising result for future applications in different engineering industries.

**KEY WORDS:** Dynamic mechanical analysis; epoxidized linseed oil; fracture toughness; impact strength; organo-montmorillonite.

## INTRODUCTION

The importance of environmentally friendly natural products for industrial applications becomes radically clear in recent years with increasing emphasis on the environmental issues, waste disposal, and depleting non-renewable resources. Renewable resource-based polymers, having new advantage of eco-friendliness, can form a platform to replace/substitute petroleum-based polymers through innovative design for the new biobased polymers which can compete or even surpass the existing petroleum-based materials on cost-performance basis with adding advantage of eco-friendliness. There is a growing urgency to develop and commercialize new bio-based products and other innovative technologies that can unhook widespread dependence on fossil fuel. As a result, the development of new biobased thermoset polymers is being accelerated [1–10].

Petroleum derived epoxy resins are known for superior tensile strength, high stiffness, excellent electrical strength, and exceptional solvent resistance. Furthermore, cured epoxy resins have good resistance to heat and chemical attack. The chief drawbacks of epoxy resins for industrial use are their brittleness and high cost. Therefore, modifying epoxy resins has been of intense research interest. A tougher, more flexible material can be obtained by incorporating a flexible epoxy resin, curing agent or reactive additives into the network during curing. Linseed oil is available abundantly across the world, and epoxidized linseed oil (ELO) is already commercially available by various companies. Such functionalized vegetable oils have found applications in coatings and plasticizer additives. More value-added applications of such epoxidized vegetable oil will give much return to agriculture, thereby reducing the burden of petroleum-based products. In addition, the blend of nanoscale reinforcements, such as organically modified montmorillonite, and biobased epoxy resin in presence of suitable curing agents would

[1] Composite Materials and Structures Center, 2100 Engineering Building, Michigan State University, East Lansing, MI 48824, USA.
[2] The School of Packaging, 130 Packaging Building, Michigan State University, East Lansing, MI 48824, USA.
[3] To whom all correspondence should be addressed. E-mail: mohantya@msu.edu

result in advanced materials potentially applicable in various industries and equipment. In the past studies, it was found that the clay nanocomposites have splendid characteristics, i.e. remarkably increased elastic modulus and fracture toughness [11–20].

This study focuses on anhydride-cured ELO epoxy resins, having high glass transition temperature. It is because the incorporation of biobased glassy epoxy resins reinforced by organically modified nanoclay would be one of the best combinations for developing environmentally friendly nanocomposites, satisfying the demanding requirements for different applications. These newly developed anhydride-cured biobased epoxy nanocomposites are characterized through thermophysical properties, Izod impact strength, and fracture toughness measurements. The thermophysical properties are evaluated by dynamic mechanical analysis (DMA). Investigation using transmission electron microscopy (TEM) is revealed excellent dispersion and exfoliation of clay nanoplatelets in biobased epoxy matrix. The morphology of the failure and fracture surfaces is observed by scanning electron microscopy (SEM) after the mechanical testing.

## EXPERIMENTS

### Materials

The main component was Epon 862, diglycidyl ether of bisphenol F (DGEBF, Resolution Performance Products, Houston TX, epoxide equivalent weight = 172). A biobased modifier, epoxidized linseed oil (ELO, Vikoflex® 7190, Atofina, Booming Prairie MN, epoxide equivalent weight = 176) replaced 20–100 wt.% of DGEBF. The mixture of DGEBF and ELO was processed with an anhydride curing agent, methyltetrahydrophthalicanhydride (MTHPA), Aradur™ HY 917 (Huntsman Advanced Materials Americas Inc., Brewster NY, equivalent weight = 159) and a 1-methylimidazole accelerator, DY 070 (Huntsman Advanced Materials Americas Inc.). The ratio by weight of the mixture of the DGEBF and ELO to the anhydride curing agent was adjusted to achieve stoichiometry. The mixing ratio was 100 parts by weight of the mixture of the DGEBA and ELO to 1.0 part accelerator.

Organo-montmorillonite clay (Cloisite® 30B, Southern Clay Products, Gonzales, TX), a natural montmorillonite modified with methyl, tallow, bis(2-hydroxyethyl) quaternary ammonium (MT2EtOH) ion, was blended in the epoxy using sonication technique. Nanocomposites were made using clay loading of 5.0 wt.%. To fabricate exfoliated clay nanocomposites, the 5.0 wt.% of organo-clay was sonicated by a sonicator (Virsonic 60, The Virtis Company Inc., Gardiner NY) in acetone for 2 hours using a solution concentration of more than 30 L of acetone to 1 kg of organo-clay, while it was constantly stirred by a magnetic stirrer. The DGEBF and the ELO were then added and mixed with a magnetic stirrer for an additional hour. The acetone was removed by vacuum extraction at approximately 100°C for 24 h, after that time the anhydride curing agent was blended in the solution with a magnetic stirrer. Intercalated clay nanocomposites were processed without sonication mentioned above; the clay particles were directly added to the mixture of DGEBF, ELO, and MTHPA, and then continuously stirred for at least 30 min. All anhydride-cured epoxy samples were cured at 80°C for 4 h followed by 160°C for 2 h.

### Characterizations

#### *Transmission Electron Microscopy*

The clay nanoplatelets in the anhydride-cured biobased epoxy matrix were observed with TEM. Thin sections of approximately 100 nm thick were obtained at room temperature by ultramicrotomy with a diamond knife having an included angle of 4°. A JEOL 2010 TEM with field emission filament in 200 kV accelerating voltage was used to collect bright field TEM images of the biobased epoxy/clay nanocomposites.

#### *Dynamic Mechanical Analysis*

Dynamic mechanical properties were collected with a TA Instruments DMA 2980 operating in the three-point bending mode at an oscillation frequency of 1.0 Hz. DMA specimens were in the form of rectangular bars of nominal 2.0 mm × 15 mm × 50 mm. Data were collected from ambient to 170°C at a scanning rate of 2°C/min. The glass transition temperature, $T_g$, was assigned as the temperature where loss factor was a maximum. A minimum of three specimens of each composition were tested.

#### *Heat Distortion Temperature*

Heat distortion temperature (HDT) was measured with a TA Instruments DMA 2980 operating in the three-point bending mode. The specimen size was

the same as the DMA specimens mentioned above. The deflection of the specimens were measured from ambient to 170°C at a scanning rate of 2°C/min under a constant load $P$. The constant load $P$ was calculated as follows:

$$P = \frac{2\sigma t^2 w}{3l} \quad (1)$$

where $\sigma$ is stress, which is 455 kN/m$^2$ as recommended in ASTM D 648 standard, $l$ is the span length between two supports in three point bending apparatus (= 50 mm), and $t$ and $w$ are the thickness and width of the specimens, respectively. The HDT was defined as a temperature at which the displacement $d$ of the specimen reached the value calculated as follows:

$$d = \frac{\varepsilon l^2}{6t} \quad (2)$$

where $\varepsilon$ is strain of the specimen (= 0.195%). A minimum of three specimens of each composition were tested to measure HDT.

### *Izod Impact Testing*

Izod impact strength was measured for biobased neat epoxy and biobased epoxy/clay nanocomposites at room temperature. Izod impact specimens with the same dimension as indicated in ASTM D256 standard were tested with a 453 g (1.0 lb) pendulum. A minimum of five specimens for each composition were tested to reduce scattering error.

### Fracture Testing

The compact tension (CT) specimens were prepared for fracture testing. The crack length $a$, the width $W$, and the thickness $B$ of the CT specimens were determined as 10, 20, and 5 mm, respectively, based on ASTM D 5045 standard. The notch was at first made by a band saw, and then the sharp initial crack tip was produced by a guillotine crack initiator and a fresh razor blade. The crack length was measured by optical microscopy after the fracture testing. The experiments were performed with a crosshead velocity of 15 mm/min to load the CT specimens. The fracture toughness was measured with at least three specimens for each different material. The critical energy release rate was calculated from the fracture toughness in plane-strain state.

### Scanning Electron Microscopy

The fracture surfaces of different biobased epoxy nanocomposites were observed with SEM. A gold coating, which is few nanometer thick, was made on the fracture surfaces to be observed. A JEOL 6300 SEM with field emission filament in accelerating voltage of 10 kV was used to collect SEM images for all samples.

## RESULTS AND DISCUSSION

### Morphology of Clay Nanoplatelets

A sample preparation scheme was used to process the modified clay in the glassy biobased epoxy network resulting in nanocomposites where the clay nanoplatelets were almost completely exfoliated by the epoxy network. Figure 1 shows both low and high magnification TEM micrographs of biobased epoxy/clay nanocomposites containing 30 wt.% ELO. A low magnification TEM micrograph (Fig. 1(a)) shows a general view of the dispersed clay nanoplatelets in the epoxy resin. In Fig. 1(a), the excellent homogeneous dispersion of clay nanoplatelets was achieved due to the clay modification with MT2EtOH and the sonication process in acetone. Figure 1(b) presents a close-up view of the completely exfoliated clay nanoplatelets in the ELO epoxy resin. In Fig. 1(b), the $d$-spacing of clay nanoplatelets cannot be identified because of the almost complete exfoliation. The perpendicular view to the $c$-axis (i.e., the parallel view along the $a$–$b$ plane) shows typical elongated fiber-like feature. The size of the clay nanoplatelets after the exfoliation was in the range between 50 and 200 nm on the $a$–$b$ plane, which is absolutely smaller than the intercalated clay nanoplatelets [21]. It is because it is easier to break completely exfoliated clay nanoplatelets, having the thickness of only 1 nm, rather than intercalated clay sticking with a number of clay layers. No difference of the clay morphology was observed regardless of different amount of ELO, since all nanocomposites were processed by the sonication technique. The excellent exfoliation was also confirmed from the measurements of wide angle X-ray scattering that did not show any diffraction peaks. These homogeneous dispersion and complete exfoliation result in the excellent improvement for elastic modulus of clay nanocomposites.

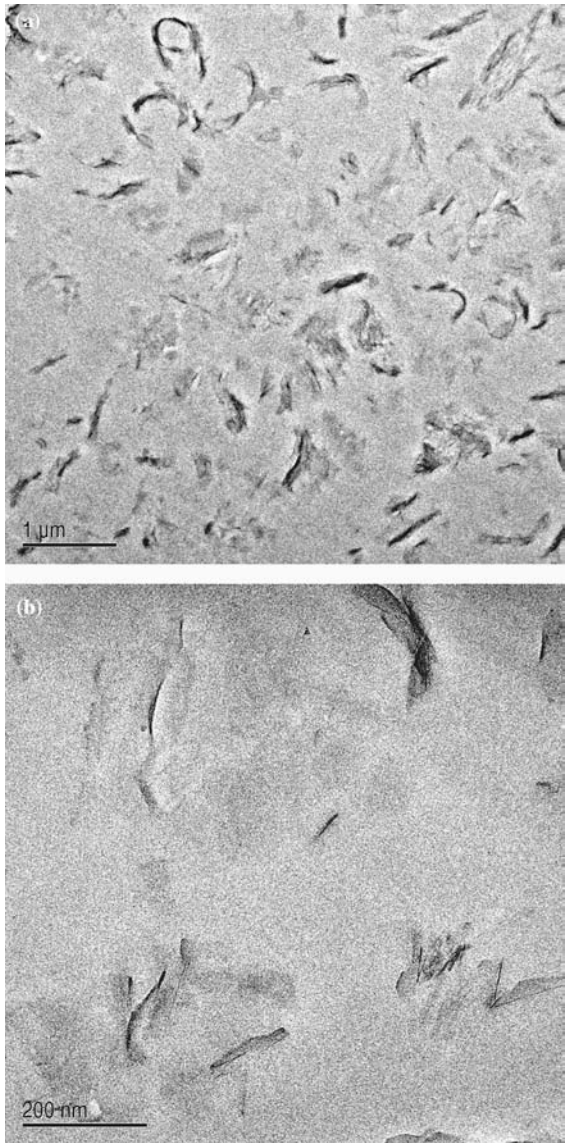


**Fig. 1.** Bright-field TEM micrographs revealing homogeneous dispersion and complete exfoliation of clay nanoplatelets in epoxy matrix containing 30 wt.% ELO. (a) Low magnification, scale bar = 1 μm; (b) high magnification, scale bar = 200 nm.

## Density of Biobased Neat Epoxy

Figure 2 shows the change of the density of the anhydride-cured ELO neat epoxy. The solid circles with standard deviations represent the experimental results and the solid line represents the least-squares fit line, respectively. The density of the ELO neat epoxy linearly decreased with increasing the amount of ELO. The result of the least squares fit was used to calculate the theoretical values of the clay volume content of the corresponding nanocomposites having

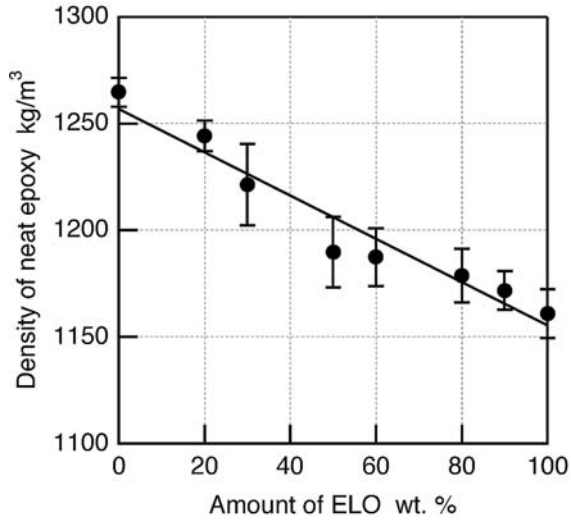


**Fig. 2.** Change of the density of biobased neat epoxy.

the same amount of ELO. The clay volume content was calculated from the density of the anhydride-cured ELO neat epoxy and density of the clay (~2.65 g/cc). The change of the storage modulus of the biobased epoxy/clay nanocomposites was evaluated by Tandon–Weng equation using the theoretical clay volume content in the following section.

## Thermophysical Properties

Figure 3 shows the temperature dependency curve of storage modulus and loss factor of anhydride-cured neat epoxy containing ELO. In Fig. 3(a), the storage modulus below the glass transition temperature decreased with increasing the amount of ELO. In Fig. 3(b), the peak position of the loss factor curves are approximately 130–140°C when up to 80 wt.% DGEBF was replaced by ELO, although the loss factor peak became broader with the addition of larger amount of ELO. In other words, no clear peak shift was observed in that range of ELO amount. On the other hand, the larger peak shift of the loss factor curve was observed when more than 90 wt.% DGEBF was replaced by ELO. These results will be further discussed with the following figures.

Figure 4 shows the change of the storage modulus of the biobased neat epoxy and its clay nanocomposites at 30°C with increasing amount of ELO as replacement for DGEBF. In Fig. 4, symbols show the experimental results of the storage modulus at 30°C regarding the amount of ELO. Empty and solid symbols are for anhydride-cured biobased neat epoxy and its 5.0 wt.% clay nanocomposites, respectively.

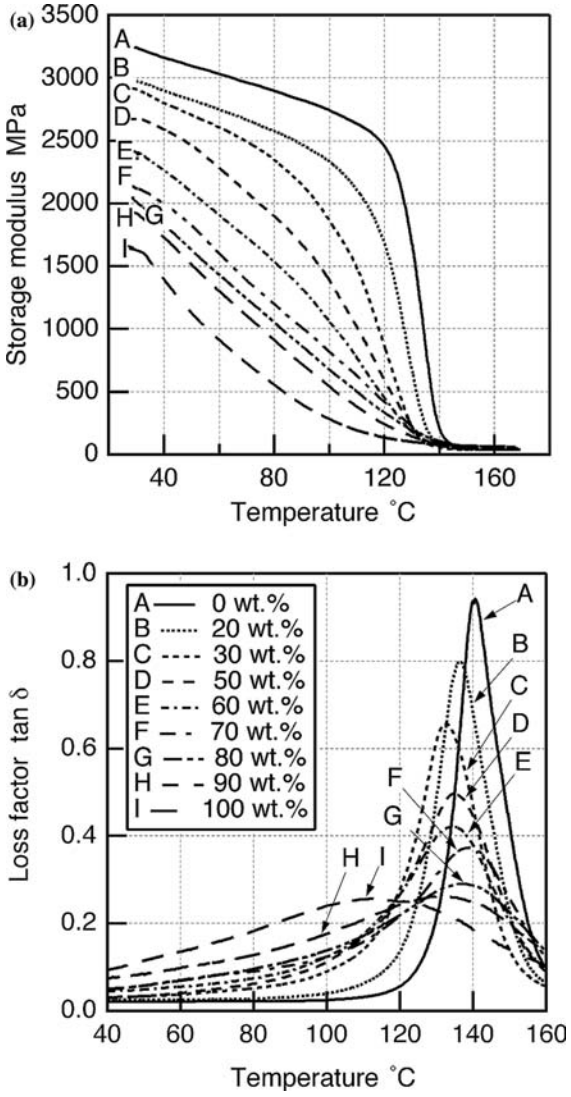


**Fig. 3.** The effect of ELO concentration for anhydride-cured neat epoxy (captions shared for both Fig. 3(a) and (b)). (a) Storage modulus; (b) loss factor.

Dashed line also shows the least squares line for neat ELO epoxy. The storage modulus of neat epoxy linearly decreased from 3.2 to 1.7 GPa with increasing amount of ELO. Therefore, it was possible to replace large amount of petroleum based DGEBF with ELO while maintaining high storage modulus, because of the selection of an anhydride curing agent. The biobased epoxy nanocomposites reinforced by 5.0 wt.% exfoliated clay exhibited a storage modulus increase at 30°C of approximately 0.72 GPa relative to the value of the biobased neat epoxy, representing up to 34.7% improvement. The intercalated clay nanocomposites showed smaller improvement than the

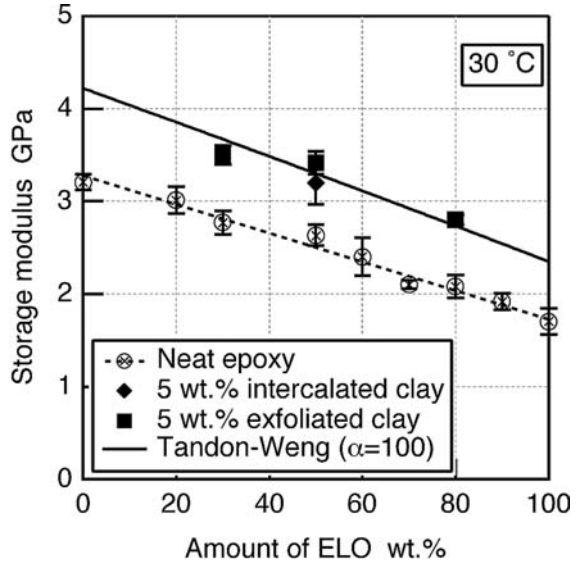


**Fig. 4.** Change in storage modulus of anhydride-cured ELO neat epoxy and its clay nanocomposites at 30°C measured by DMA.

exfoliated clay nanocomposites. This reinforcing effect can be theoretically calculated with Tandon–Weng equation [22] for 3-D randomly oriented flake-reinforced composites. Organic content in the organo-montmorillonite has been measured as 28.5 wt.% by thermogravimetric analysis (TGA). Therefore, when 5.0 wt.% organo-clay was added to the biobased epoxy, it was regarded as adding 3.57 wt.% neat clay to the biobased epoxy. Consequently, the volume percent of the clay nanoplatelets was calculated as approximately 1.6 vol.% using the densities of clay (2.65 g/cm$^3$) and the experimental value of the density of different biobased neat epoxy. The quantity of a ternary ammonium salt in the organo-clay was extremely small comparing the quantity of the biobased epoxy matrix. Therefore, the change of the density of the biobased epoxy matrix of the clay nanocomposites was ignored; the density of the ternary ammonium salt was regarded as the same as the density of epoxy matrix. The modulus of clay nanoplatelets was considered as 170 GPa [23]. Using a sensitivity approach, an average value of the aspect ratio of the exfoliated clay nanoplatelets was estimated. The least square fit line for the storage modulus of the neat ELO shown in Fig. 2 was used to evaluate the storage modulus of 1.6 vol.% exfoliated clay nanocomposites. The theoretical prediction from 3-D Tandon–Weng equation shown in Fig. 4 was computed with an aspect ratio of 100, yielding an extremely close fit to the experimental data acquired

by DMA. This theoretically estimated aspect ratio was absolutely close to the observed value as discussed in Fig. 1(b).

Figure 5 shows the relation between the glass transition temperature ($T_g$) determined from the peak position of loss factor curve and the amount of ELO for anhydride-cured neat epoxy and its 5.0 wt.% exfoliated clay nanocomposites. The relation for the anhydride-cured ELO neat epoxy was not linearly correlated; the $T_g$ slightly decreased with increasing amount of ELO up to 50 wt.%, then $T_g$ increased with increasing amount of ELO up to 80 wt.%. The sample of anhydride-cured 100% ELO showed approximately 110°C as the lowest $T_g$. Like anhydride-cured petroleum-based epoxy/clay nanocomposites, which was previously studied by some of the present authors, the glass transition temperature of ELO epoxy/clay nanocomposites decreased because of the quaternary ammonium ion used for clay modification. The clay nanoplatelets used in this study were organically modified, and the organic content, MT2EtOH, was approximately 28.5% by weight. The decrease in $T_g$ is due to the plasticization effect of quaternary ammonium ion in organo-montmorillonite in anhydride-cured epoxy system, resulted in the lower closs-link density of anhydride-cured epoxy matrix. A long-chain fatty alkyl amine, such as the methyl, hydroxyethyl, tallow-alkyl amine, was released from the organo-clay through simple thermal dissociation during curing. Such a low molecular weight fatty-alkyl amine could readily act as a plasticizer, and hence, lower glass transition temperature was obtained when more organo-clay was added to the anhydride-cured epoxy system. It was already observed that the composites with the organo-montmorillonite clay could be cured with only MTHPA without adding any accelerator, and this nanocomposite sample without the accelerator showed even lower glass transition temperature, although the neat anhydride-epoxy mixture did not polymerize without the accelerator.

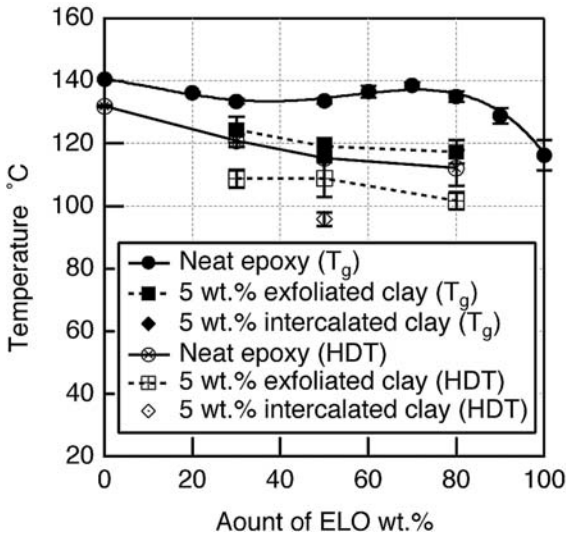


**Fig. 5.** Change in glass transition temperature and HDT of anhydride-cured ELO neat epoxy and its clay nanocomposites measured by DMA.

As discussed in Fig. 3(b), the peak of loss factor curve was broadened when more ELO replaced DGEBF. This might result in the inaccurate determination of $T_g$. Therefore, HDT was also measured to understand the maximum temperature at which the biobased epoxy can be applied as a rigid material. Figure 5 shows the change of HDT with respect to the amount of ELO before and after adding 5.0 wt.% exfoliated organo-clay. Differently from $T_g$, HDT of the ELO neat epoxy linearly decreased with increasing the amount of ELO. The HDT of 80 wt.% ELO was still higher than 100°C. Since $T_g$ decreased with increasing clay content as shown in Fig. 4, HDT value also decreased after adding organo-clay nanoplatelets. For the automotive and aeronautical applications, it should be noted that HDT of minimum of 100°C is required. Therefore, it could be thought that the maximum of 50 wt.% ELO might be suitable to process clay nanocomposites to maintain high HDT value.

Figure 6 shows the relation between peak factor of loss factor curve and the amount of ELO of anhydride-cured epoxy system. The peak factor is defined as the value of full-width at half maximum (FWHM) divided by the height of the peak. This parameter can give a qualitative assessment of the homogeneity of the epoxy network and the distribution of the molecular weight. Therefore, the broader peak is reflected on the larger value of the peak factor. Empty and solid marks show the results of neat epoxy and its 5.0 wt.% exfoliated clay nanocomposites, respectively. Broken and solid lines also show the least squares lines for neat epoxy and its 5.0 wt.% exfoliated clay nanocomposites, respectively. As can be seen in this figure, the peak factor of neat ELO epoxy radically increased with increasing the amount of ELO. Especially in comparing 100% DGEBF and 100% ELO neat epoxy, the difference of the peak factor was almost 2 orders of magnitude. This suggests that biobased epoxy has broadened glass transition region because of heterogeneous ELO epoxy polymer network, although the phase separation

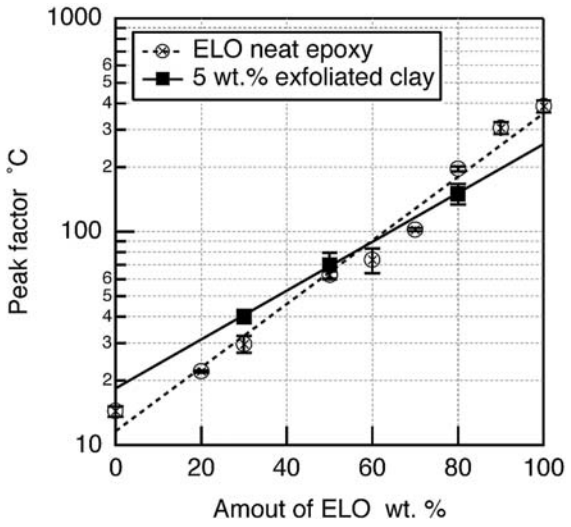


**Fig. 6.** Peak factor of loss factor curves of anhydride-cured ELO neat epoxy and its clay nanocomposites.

was not observed in the following SEM micrographs. Hence, to determine $T_g$, as discussed in Fig. 5, using broadened loss factor curve may include inaccuracy. The poor homogeneity of the biobased epoxy network is due to the ELO produced from natural resources consisting of multiple constituents. Interestingly, the peak factor of 80 wt.% ELO sample became smaller after adding 5.0 wt.% exfoliated clay nanoplatelets. This fact suggests that the excellent dispersion of exfoliated clay nanoplatelets improved homogeneity of polymer network, which can be confirmed by the smaller value of peak factor. For anhydride-cured ELO epoxy/clay nanocomposites, it can be thought from the cross section of 2 least squares lines that this homogeneity improvement effect due to exfoliated clay nanoplatelets is possible when more than 60 wt.% ELO was added. This improvement may also suggest that the uniform dispersion of exfoliated clay platelets can avoid phase separation which is observed in epoxy containing different vegetable oils.

## Izod Impact Strength

Figure 7 shows the change of Izod impact strength of anhydride-cured neat epoxy with different amount of ELO before and after adding 5.0 wt.% exfoliated clay nanoplatelets. The anhydride curing agent process rigid epoxy sample having high cross-link density, therefore, the value of Izod impact strength was relatively low. As seen in Fig. 7, the Izod impact strength of anhydride-cured neat ELO epoxy was constant, although the amount of ELO was changed. This also suggests that the glassy epoxy materials, having high glass transition temperature, were obtained even when the large amount of DGEBF was replaced by ELO, since rubbery epoxy materials, having low glass transition temperature, show much higher Izod impact strength [24]. For rigid epoxy system, it was reported that it is difficult to maintain the same value of Izod impact strength and that the impact strength was independent from the clay morphology [25]. Although no difference was observed between intercalated and exfoliated clay nanocomposites in Fig. 7, the Izod impact strength could be maintained or become even slightly higher after the exfoliated clay platelets were added to ELO epoxy system, as the average value of all sample is indicated in Fig. 7.

Figure 8 shows SEM micrographs of impact failure surfaces of anhydride-cured biobased neat epoxy containing 50 wt.% ELO and its 5.0 wt.% exfoliated clay nanocomposites. In Fig. 8(a), the failure surface of the anhydride-cured ELO neat epoxy was extremely flat. This suggests that the behavior of the anhydride-cured ELO neat epoxy was elastic and the crack was propagated straightforward under the impact loading, although several small pieces of resin were found on the failure surface. The phase separation was not observed, either. Therefore, DGEBF, ELO, and MTHPA were homogeneously mixed and then cured. Similar morphology was observed for anhydride-cured

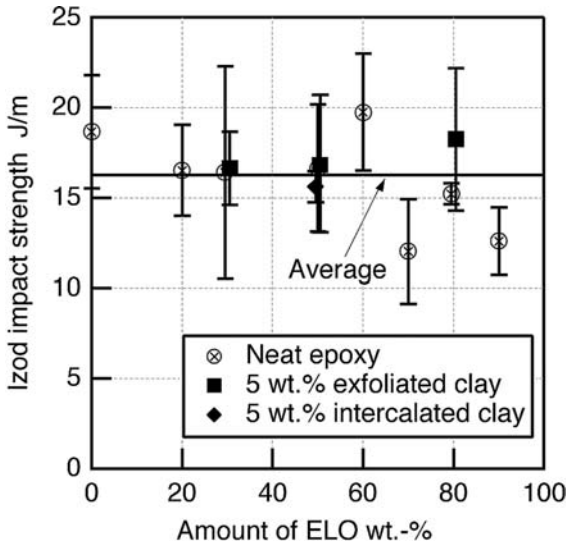


**Fig. 7.** Change in Izod impact strength of anhydride-cured neat epoxy with ELO and its clay nanocomposites.

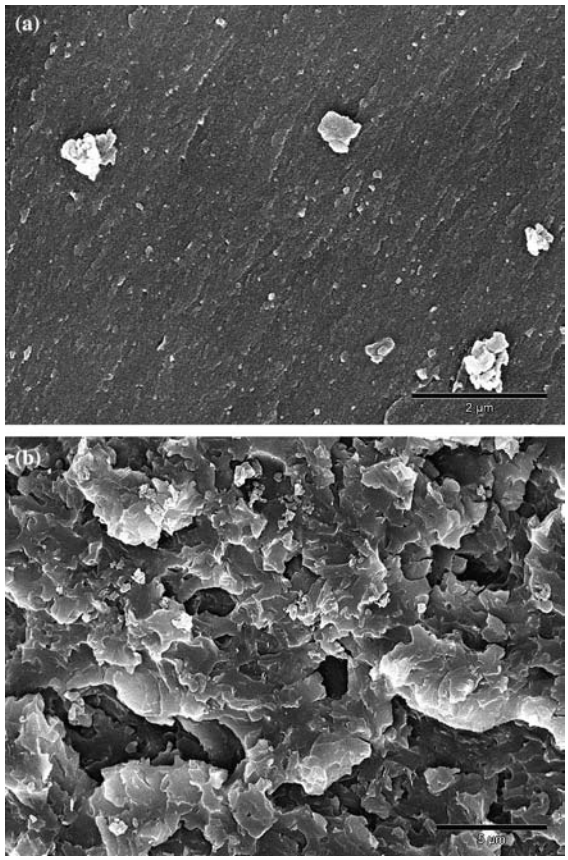


**Fig. 8.** SEM micrographs of impact failure surfaces: (a) ELO neat epoxy, scale bar = 2 μm; (b) 5.0 wt.% exfoliated clay nanocomposites, scale bar = 5 μm.

DGEBF and all other biobased epoxy containing different amount of ELO. The lack of the phase separation resulted in as relatively low Izod impact strength as that of anhydride-cured DGEBF. In Fig. 8(b), the failure surface of biobased epoxy nanocomposites, containing 50 wt.% ELO and reinforced by 5.0 wt.% exfoliated clay nanoplatelets, showed the rougher surface. Since phase separation was not observed on the impact failure surface after adding clay nanoplatelets, there was no difference of the Izod impact strength between anhydride-cured ELO neat epoxy and its clay nanocomposites.

## Fracture Testing

Non-linearity was seldom observed in load-displacement diagrams of biobased neat epoxies and their nanocomposites. Therefore, the maximum load was used to evaluate fracture toughness. Figure 9 shows the fracture toughness of the anhydride-cured DGEBF, biobased neat epoxy containing 50 wt.% ELO, and its 5.0 wt.% exfoliated and intercalated clay nanocomposites. As seen in Fig. 9, the anhydride-cured ELO neat epoxy showed almost the same value as the fracture toughness of the anhydride-cured DGEBF epoxy. For biobased epoxy/clay nanocomposites, the intercalated clay nanocomposites showed higher fracture toughness than the exfoliated clay nanocomposites.

The fracture properties can also be discussed with critical energy release rate as shown in Fig. 10. The anhydride-cured neat ELO epoxy has slightly smaller storage modulus than the DGEBF as discussed in Fig. 4. Therefore, the critical energy release rate of the anhydride-cured ELO neat epoxy was slightly higher than that of the DGEBF. After adding 5.0 wt.% intercalated clay nanoplatelets, the critical energy release rate was greatly improved, although that after adding 5.0 wt.% exfoliated clay nanoplatelets showed slight improvement, comparing with the ELO neat epoxy. The reason of the different critical energy release rate is explained with SEM micrographs.

Figure 11 shows the SEM micrographs of the fracture surfaces of the anhydride-cured ELO neat epoxy and its 5.0 wt.% exfoliated and intercalated clay nanocomposites. In Fig. 10(a), the fracture surface of the ELO neat epoxy was completely flat. This suggests that the anhydride-cured ELO neat epoxy is brittle and the load-displacement diagram was almost completely elastic. Hence, the crack propagated straightforward and the minimal fracture surface area was created by the crack propagation. Minimal fracture surface area means minimal consumption of

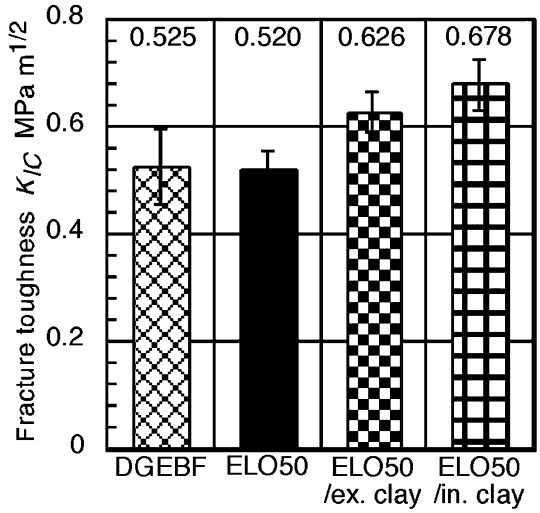


**Fig. 9.** Change in fracture toughness of anhydride-cured neat epoxy with ELO and its clay nanocomposites.

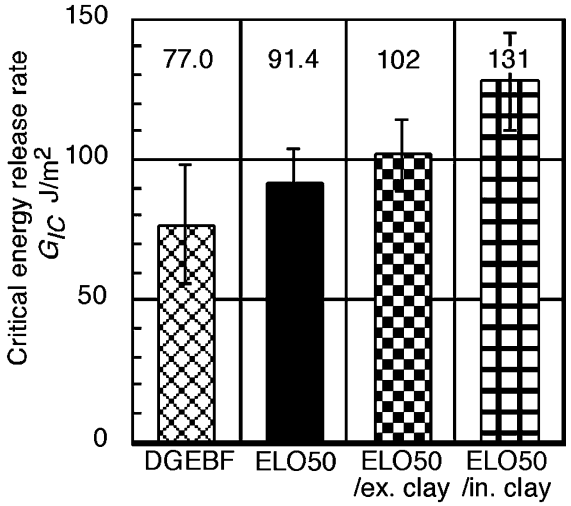


**Fig. 10.** Change in critical energy release rate of anhydride-cured neat epoxy with ELO and its clay nanocomposites.

the energy for crack propagation. Figure 11(b) and (c) show the fracture surfaces of ELO/exfoliated clay and ELO/intercalated clay nanocomposites, respectively. The surface roughness of intercalated clay nanocomposites is obviously larger than that of exfoliated clay nanocomposites. For intercalated clay nanocomposites, the crack tends to avoid reaching the aggregations of intercalated clay particles, since the adhesion at the biobased epoxy/clay interface was excellent and the strength of clay aggregation prevents crack from propagating [25]. Therefore, the crack tends to curve in micron order, and this results in the higher critical energy release rate with the rougher fracture surface. On the other hand for exfoliated clay nanocomposites, it is easy to break each individual clay nanoplatelets because of the thin size as 1 nm, which is not strong enough to prevent the crack from propagating. Smaller inclusions are less effective for prevention of the crack propagation. Griffith explained the fracture criteria that the crack is propagated when the strain energy reaches the certain value, which can newly create the fracture surface. In other words, when the fracture surface area is larger, more strain energy is necessary. Consequently, the fracture surface area is larger when the critical energy release rate is larger. Indeed, the critical energy release rate was greatly improved with the intercalated clay nanoplatelets as discussed in Fig. 10.

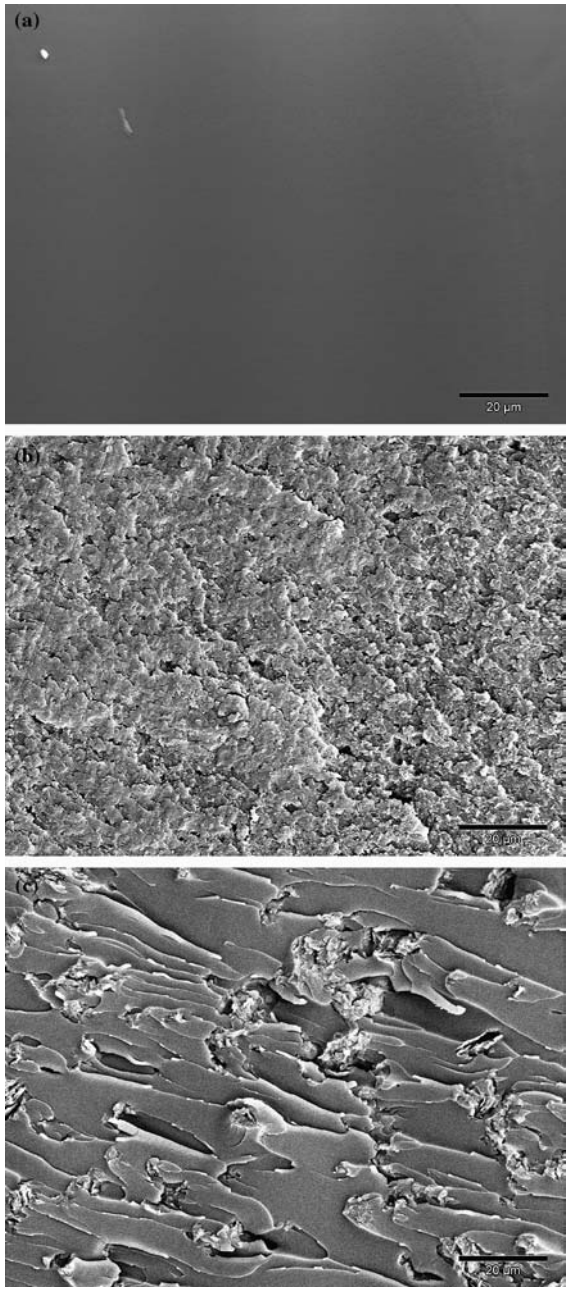


**Fig. 11.** SEM micrographs of fracture surfaces: (a) ELO neat epoxy, scale bar = 20 μm; (b) 5.0 wt.% exfoliated clay nanocomposites, scale bar = 20 μm; (c) 5.0 wt.% intercalated clay nanocomposites, scale bar = 20 μm.

## CONCLUSIONS

In this paper, the new biobased epoxy materials and their clay nanocomposites were processed with DGEBF, ELO, and MTHPA, and the thermophysical and mechanical properties of these samples were discussed. The storage modulus, glass transition temperature, and HDT decreased with increasing amount of ELO, which replaced the same amount of DGEBF. Sonication technique was used to process

the organically modified clay nanoplatelets in the glassy biobased epoxy network resulting in nanocomposites where the clay nanoplatelets were almost completely exfoliated and homogeneously dispersed in the biobased epoxy network. The processed exfoliated clay nanocomposites showed higher storage modulus comparing with the neat epoxy containing the same amount of biobased modifier, and the reinforcing effect of the exfoliated clay nanoplatelets was evaluated with 3-D Tandon–Weng equation. After 5.0 wt.% organo-clay was added to the biobased epoxy, the glass transition temperature and the HDT additionally decreased. The decrease was because of the plasticizing effect of the organic content of the organo-clay. Izod impact strength was constant with changing the amount of ELO and adding clay nanoplatelets. No phase separation was observed for all neat epoxy and its clay nanocomposites, and this resulted in relatively low Izod impact strength. The fracture toughness and the critical energy release rate of epoxy were greatly improved with the addition of intercalated clay. This was correlated to the rougher fracture surface observed by SEM.

## ACKNOWLEDGMENTS

The authors are grateful to National Science Foundation Partnership for Advancing Technologies in Housing (NSF-PATH) 2001 Award No. 0122108 for partial financial support and Michigan State University's Research Excellence Fund for partial financial supports. The authors are also thankful to Atofina, Booming Prairie MN, and Huntsman Advanced Materials Americas Inc., Brewster NY, for supplying samples.

## REFERENCES

1. S. Dirlikov, I. Frischinger, and Z. Chen (1996) *Adv. Chem. Ser.* **252**, 95–109.
2. D. Ratna and A. K. Banthia (2000) *J. Adhesion Sci. Eng.* **14(1)**, 15–25.
3. D. Ratna (2001) *Polym. Int.*, **50**, 179–184.
4. F. Li and R. C. Larock (2001) *J. Polym. Sci. Part B Polym. Phys.* **39**, 60–77.
5. E. Can, S. Kusefoglu, and R. P. Wool (2001) *J. Appl. Polym. Sci.* **81**, 69.
6. S. N. Khot, J. J. LaScala, E. Can, S. S. Morye, G. I. Williams, G. R. Palmese, S. H. Kusefouglu, and R. P. Wool (2001) *J. Appl. Polym. Sci.* **82**, 703–723.
7. L. K. Belcher, L. T. Drzal, M. Misra, and A. K. Mohanty (2002) *Polym. Mater.: Sci. Eng.* **87**, 256–257.
8. G. Mehta, M. Misra, L. T. Drzal, and A. K. Mohanty (2003) *Proc. 14th International Conference on Composite Materials*, July 14–18, CD-ROM #1754.
9. R. P. Wool, S. N. Khot, J. J. LaScala, S. P. Bunker, J. Lu, W. Thielemans, E. Can, S. S. Morye, and G. I. Williams (2002) in *ACS Symposium Series 823* (Advancing Sustainability through Green Chemistry and Engineering), pp. 177–204.
10. H. Miyagawa, A. K. Mohanty, M. Misra, and L. T. Drzal (2004) *Macromolecular Materials and Engineering* **289**, 629–635.
11. P. C. LeBaron, Z. Wang, and T. J. Pinnavaia (1999) *Appl. Clay Sci.* **15**, 11–29.
12. P. B. Messersmith and E. P. Giannelis (1994) *Chem. Mater.* **6**, 1719–1725.
13. T. Lan and T. J. Pinnavaia (1994) *Chem. Mater.* **6**, 2216–2219.
14. C. Zilg, R. Muelhaupt, and J. Finter (1999) *Macromol. Chem. Phys.,* **200(3)**, 661–670.
15. A. Lee and J. D. Lichtenhan (1999) *J. Appl. Polym. Sci.* **73**, 1993–2001.
16. J. M. Brown, D. Curliss, and R. A. Vaia (2000) *Chem. Mater.* **12**, 3376–3384.
17. A. S. Zerda and A. J. Lesser (2001) *J. Polym Sci.: Part B: Polym. Phys.* **39**, 1137–1146.
18. X. Kornmann, R. Thomann, R. Muelhaupt, J. Finter, and L. Berglund (2002) *J. Appl. Polym. Sci.* **86**, 2643–2652.
19. X. Kornmann, R. Thomann, R. Muelhaupt, J. Finter, and L. Berglund (2002) *Polym. Eng. Sci.* **42**(9), 1815–1826.
20. H. Miyagawa, M. J. Rich, and L.T. Drzal (2005) *Polymer Composites* **26**, 42–51.
21. H. Miyagawa, W.-A. Chiou, and I. M. Daniel (2001) *Microscopy and Microanalysis, vol. 7 (suppl. 2), Proceedings: Microscopy & Microanalysis 2001*, Long Beach CA, pp. 946–947.
22. G. P. Tandon and G. J. Weng (1986) *Composites Sci. Technol.* **27**, 111–132.
23. D. Shia, C. Y. Hui, S. D. Burnside, and E. P. Giannelis (1998) *Polym. Composites*, **19**(5), 608–617.
24. H. Miyagawa, M. J. Rich, and L. T. Drzal (2003) *31st Annual Conference of North American Thermal Analysis Society (NATAS)*, Albuquerque NM, #109 (CD-ROM).
25. H. Miyagawa and L. T. Drzal (2004) *Journal of Adhesion Science and Technology* **18**, 1571–1588.